Published in final edited form as:
Cephalalgia. 2011 September ; 31(12): 1254–1265. doi:10.1177/0333102411408360.

Sodium MRI in a rat migraine model and a NEURON simulation study support a role for sodium in migraine

Michael G Harrington[1], **Eduard Y Chekmenev**[2], **Victor Schepkin**[3], **Alfred N Fonteh**[1], and **Xianghong Arakaki**[1]

[1]Huntington Medical Research Institutes, USA

[2]Vanderbilt University Institute of Imaging Science, USA

[3]Florida State University, USA

Abstract

Introduction—Increased lumbar cerebrospinal fluid (CSF) sodium has been reported during migraine. We used ultra-high field MRI to investigate cranial sodium in a rat migraine model, and simulated the effects of extracellular sodium on neuronal excitability.

Methods—Behavioral changes in the nitroglycerin (NTG) rat migraine model were determined from von Frey hair withdrawal response and photography. Central sensitization was measured by counting cFos-immunoreactive cells in the trigeminal nucleus caudalis (TNC). Sodium was quantified in vivo by ultra-high field sodium MRI at 21 Tesla. Effects of extracellular sodium on neuronal excitability were modeled using NEURON software.

Results—NTG decreased von Frey withdrawal threshold (p=0.0003), decreased eyelid vertical height:width ratio (p<0.0001), increased TNC cFos stain (p<0.0001), and increased sodium between 7.5 and 17% in brain, intracranial CSF, and vitreous humor (p<0.05). Simulated neurons exposed to higher sodium have more frequent and earlier spontaneous action potentials, and corresponding earlier sodium and potassium currents.

Conclusions—In the rat migraine model, sodium rises to levels that increase neuronal excitability. We propose that rising sodium in CSF surrounding trigeminal nociceptors increases their excitability and causes pain and that rising sodium in vitreous humor increases retinal neuronal excitability and causes photosensitivity.

Keywords

Sodium MRI; photophobia; central sensitization; cerebrospinal fluid; nitroglycerin; rat migraine model

Introduction

Migraine affects 30 million Americans (1) and is typified by episodes that last hours to days. Symptoms include severe headache, nausea, cognitive impairment, and discomfort from

Corresponding author: Michael G Harrington, Molecular Neurology Program, Huntington Medical Research Institutes, 99 North El Molino Avenue, Pasadena, CA 91101, USA, mghworks@hmri.org.

Declaration of competing interests

None.

normal light, sound and smells (2). The primary neurons of migraine pain are located in the trigeminal ganglion; secondary neurons in the brain stem trigeminal nucleus caudalis (TNC) send fibers to the thalamus, while third-order neurons project to the cortex (3). In photophobia, nociceptive cortico- thalamic neurons are modulated by retinal ganglion cell projections (4). The clinical features of migraine reflect distinct and widespread deviations from normal neuronal excitability in these pathways, but the mechanism for the altered excitability remains elusive and is the focus of this work.

The leading candidates to alter neuronal excitability stem from ionic disturbances that arise from the phenomenon of cortical spreading depression (CSD) and/ or from genetic variation, though conclusive evidence is lacking for both of these in the primary migraine symptoms. CSD is considered the basis for the migraine aura (5,6) and can activate the rat trigeminovascular system (7–9), however most migraineurs do not experience aura (2). CSD may be the silent trigger in these cases without aura symptoms, or CSD may not be the trigger for migraine (10). Genetic studies of familial hemiplegic migraine (FHM), a rare migraine subgroup, indicate an ionic disturbance (11), but FHM mutations have not been found in common migraine (12).

We recently sought evidence for ionic disturbance in migraine that might directly affect neuronal excitability. Sodium levels were increased during migraine in lumbar cerebrospinal fluid (CSF) but not in blood, while potassium, calcium, and magnesium were not altered in CSF or blood (13). Brain interstitial fluid and CSF are in direct communication (14), and sodium moves from intracranial to lumbar regions within minutes (15). Assuming intracranial CSF is the source of the increased lumbar CSF sodium in migraine, we expect intracranial sodium levels will be higher, because any addition to intracranial sodium will be diluted in the larger volume of spinal fluid.

This hypothesis is difficult to test because of the invasiveness of intracranial CSF sampling, so we sought to employ non-invasive sodium MRI, which has unique MR properties and challenges compared to ^{1}H MRI. Sodium has only one stable isotope, ^{23}Na, which has a relatively low gyromagnetic ratio (γ) with respect to that of protons (^{1}H), with $\gamma_{1H}/\gamma_{23Na}$=3.78. The decrease in sensitivity due to this low γ is partially offset because ^{23}Na is quadrupolar with a nuclear spin value, I_{23Na}=3/2, compared to I_{1H}=½; because MRI sensitivity scales as $I\bullet(I+1)\bullet\gamma^{3}$, ^{23}Na is only 10.8 times less sensitive than ^{1}H. Moreover, ^{23}Na differs in MR relaxation properties, allowing for ~50 times faster image acquisition compared to that of ^{1}H in tissue water. Despite this nominal sensitivity argument, biological and human ^{23}Na MRI has been largely unexplored because of two primary difficulties. First, physiological levels of sodium are approximately three orders of magnitude lower than those of protons. This fundamental sensitivity barrier of low spin density causes low spatial resolution. Second, fast spin-spin (T_2) relaxation on the time scale of a few milliseconds for in vivo ^{23}Na puts strict time requirements in sodium MRI sequences. As a consequence, ultra-short echo time (UTE) sequences are used for in vivo sodium MRI.

Because even the high-field MRI at 9.4 Tesla (T) has spatial resolution of several mm^3 and relatively low signal-to-noise ratio (16) (SNR), we used the ultra-high magnetic field of 21.1T (17) with a custom, volume head radiofrequency (RF) coil (18), designed for dual channel imaging (^{1}H and ^{23}Na) at 900 MHz, and with capability for anesthesia, pulse, blood pressure, and temperature monitoring. We tested if sodium is altered in the nitroglycerin (NTG)-induced central sensitization that is used widely for migraine research (19–22). We also tested how elevated extracellular sodium affected neuronal excitability in simulated neurons.

Materials and methods

Animals

Animals were housed in pairs on Lab Paperchip pellets in a temperature and humidity-controlled room, under a 12-h light–dark cycle with lights off at 18:00 hours. Water and Purina rodent lab chow was provided ad libitum. Animal procedures were approved by the Institutional Animal Care and Use Committees at Huntington Medical Research Institutes (HMRI) in Pasadena, CA, and at the National High Field Magnetic Field Laboratory (NHMFL) in Tallahassee, FL. A total of 37 Sprague-Dawley male rats (Harlan) between 180 and 240 g in weight were used in these studies.

Behavioral studies and immunohistochemistry—Animals were acclimated to their study boxes (IITC Life Science) for at least 1 hour, followed by baseline testing of hind paw withdrawal. They received intraperitoneal injection of either NTG (10 mg/kg) or saline (same volume as NTG), following which they were tested hourly. Von Frey hair testing was the most robust behavioral measure; we determined that body grooming, pinprick, and cranial testing were too variable. Because NTG-treated rats appeared to squint their eyes, three NTG- and three saline-injected animals were photographed in alternating order and at the same distance from the camera. Photography was repeated after a few minutes, within 40–45 minutes post-injection. The inter-eyelid, height-to-width ratio was measured for each animal on these images.

Three and a half hours after intra-peritoneal (ip) injections, rats were deeply anesthetized with pentobarbital (50–100 mg/kg), followed by transcardial perfusion with ~200mL of saline until the venous return was clear of blood, and by 200mL of 2% paraformaldehyde in PBS. Brains were removed, post-fixed overnight, cryoprotected by soaking in 30% sucrose in PBS for two days, frozen, and sliced into 40 μm sections using a cryostat (Mikron). For immunostaining of cFos, free-floating brain sections were pre-incubated for 1 h with 0.01M PBS containing 0.5% Triton X- 100 and 5% normal goat serum, incubated for 2 hours with rabbit primary antibody to cFos (1:500 dilution, Santa Cruz Labs) and incubated for 2 hours with goat anti-rabbit, biotinylated secondary antibody. Each step was preceded and followed by washes in 0.01M PBS. After incubation with ABC complex (Vector Labs), slices were rinsed in PBS and cFos was detected using the DAB chromogen (Biogenex). TNC regions were identified with reference to the Paxinos and Watson brain atlas (23).

Sodium and proton MRI at 21.1 T

For in vivo MRI, animals were anesthetized with 2% isoflurane and their eyes were protected with Puralube® vet ointment. NTG (10 mg/kg) or saline ip injections were administered immediately before entry to the MRI probe. Anesthesia was maintained with isoflurane for up to 4 hours in the probe in which they were strapped vertically, with monitoring of respiration and temperature. The isoflurane was adjusted to 1.5– 2.5% to maintain a stable respiration between 50 and 70 rpm during the anesthetic and imaging. Most animals were euthanized with CO_2 after the MRI. To study the serial effects of NTG, three animals were allowed to recover when removed from the imaging probe and the anesthetic and returned healthy to cages for 3–4 days before repeat imaging. Timing of all scans was recorded in relation to the injections. Placing the rat, shimming, and acquiring a reference-proton MRI scan delayed the start of the first 21-min ^{23}Na MRI scan approximately 5 minutes after injection. ^{23}Na MRI scans were taken for each treatment (no injection, saline, or NTG injection). On some occasions, rats had up to six ^{23}Na MRI sequence repetitions in a study. At the completion of each ^{23}Na MRI series, a high-resolution proton MRI was performed (5 min).

We used the vertical, unshielded 21.1 T magnet, designed and constructed at the NHMFL, Tallahassee, FL (17,24). It has a warm bore of 105 mm. Additionally it has a shielded gradient coil with ID=64mm and an 18-channel room-temperature shimming insert, both made by Resonance Research, Inc., Billerica, MA. Shimming creates a homogeneous area for ^{23}Na MRI with a diameter of ~40mm and length of ~50 mm. This magnet is equipped with a Bruker Avance III console operated by ParaVision 5.1, performing sodium and proton MRI at 237/ 900 MHz. A double-tuned ^{23}Na/^{1}H RF coil was used in this study, allowing for the acquisition of anatomical proton images and functional sodium MR images without any change in animal position.

Rat sodium MR images were acquired using a 2D ultra-short echo time MRI pulse sequence, which is a part of the Bruker imaging software. Field of view (FOV) was 64mm and slice thickness was 7.0 mm. The ^{23}Na MRI slice was positioned using the proton reference image. Short echo time TE=0.2 ms allowed detection of the majority of the sodium signal from intra- and extracellular components. The other imaging parameters included 128 complex points in RO direction and a total of 402 profiles were acquired using SW=30 kHz, TR=100 ms, NA=32, resulting in a scan time of 21 min. Resolution of the sodium images was ~0.5mm×0.5mm×7.0 (slice thickness) mm.

Anatomical proton reference images were acquired once for each animal using multi-slice, gradient-echo pulse sequence (FLASH, Bruker) with the following parameters: gauss slice selective RF pulse (30 degrees), TR=600.95 ms, TE=2.806 ms, SW=50 kHz, slice thickness=0.407 mm, FOV=34×34 mm, resolution in plane 0.133×0.133 mm, four averages, number of coronal slices=25, scan time 5 minutes.

^{23}Na MRI analysis

Anatomical variations in the ^{23}Na MRI were identified by approximate correlation with the most obvious change of structures in the high-resolution proton MRI after viewing these images in AVISO software and scrolling the 7mm deep ^{23}Na image through the 0.4mm deep proton images. The partial volume effect in 7mm slabs of the ^{23}Na image cannot be overcome in these first-of-a-kind 2D experiments; 3D ^{23}Na experiments are being developed to overcome this effect. The data in the reported difference images and the quantitative ROIs is, however, reproducible, while reflecting an average of all underlying structures in the 7mm slab. Difference images were computed using the algebra algorithm of the Utilities/image calculator functions in MIPAV [http://mipav.cit.nih.gov, Version 5.0.0 (2010-07-09)]. A calibration curve was constructed by applying the same 21-minute ^{23}Na MRI scan to monosodium glutamate solutions ranging from 0 to 200mM. Regions in each standard solution image similar to the location and size of the rat brain were selected using MIPAV; average voxel intensities of these regions were plotted against known concentrations of sodium after corrections for the difference in RF coil quality factor Q and for the difference between in vitro and in vivo ^{23}Na T_1 relaxation time. The percent change of sodium by NTG for the eight regions (%Δ in Table 1) was calculated from the ratio of the averaged voxel intensity from the sum of two consecutive 21-minute ^{23}Na MRIs from six rats after NTG injection divided by the sum of two consecutive ^{23}Na MRIs from six rats immediately before NTG.

Statistical methods

The difference of threshold for hind-paw withdrawal between NTG- and saline-treated rats was analyzed using a repeated-measures analysis with an unstructured covariance matrix using PROC MIXED in SAS v9.2 (SAS Institute, Cary, NC). Sodium average intensities in the same region of control- or NTG-treated rats were compared by the Kruskal–Wallis test,

two-tailed, with significance sought at the 0.05 level, and specific comparisons were made using Dunn's multiple comparison test.

Modeling

Simulations were conducted with NEURON software (25) running on a PC desktop. To build a cell model, we constructed a simple soma from a representative cylinder (diameter 20 μm; length 20 μm) and a 50 μs time step (equations are given in the Appendix). The model cell soma includes sodium current, potassium currents (delayed rectifier, K_{dr}, and A-type, K_A) (26), leak current, Na,K-ATPase, and sodium diffusion (27). The intracellular resistance, R_a, was defined as 150 Ω.cm; membrane capacitance, C_m, as $1\mu F.cm^{-2}$, and the resting membrane potential was defined as −65 mV. In the following equations, v is in mV, currents are in $mA.cm^{-2}$, and τ(time constant) is in ms. Temperature was defined to be 24°C for all simulations. The change in AP firing rate from 145mM to 160mM sodium was calculated as $\frac{Rate(160)-Rate(145)}{Rate(145)} * 100\%$.

Results

Behavioral and molecular effects of nitroglycerin

The von Frey hair-withdrawal threshold was reduced in NTG-injected (n=5) compared to saline-injected (n=5) rats at all times during our 3-hour testing (p=0.0003), as shown in Figure 1a.

We observed that rats were notably and reproducibly squinting their eyes in ambient light shortly after NTG, as seen in Figure 1b and c. The gap between eyelids was more than twice as big in saline-injected compared to NTG-injected rats when recorded on two occasions at 40 and 45 minutes after injection, p<0.0001: Eyelid height:width ratio in saline rats was 0.56, SD 0.02, n=3; eyelid height:width ratio in NTG rats was 0.25, SD 0.03, n=3.

Rat brains were removed 3.5 hours after injection; cFos immunoreactivity was increased by 2.2 fold in the trigeminal nucleus caudalis (TNC) in NTG-injected (Figure 1e) compared to saline-injected (Fig. 1d) rats, consistent with published reports (19,20). The mean number of TNC cFos stained nuclei in saline rats (n=5) was 80 (SEM 14) versus 178 (SEM 8) in NTG rats (n=5), p<0.0001, unpaired, two-tailed, t-test.

Sodium MRI and the effect of intraperitoneal nitroglycerin

We used a slice thickness of 7mm to achieve the best inplane spatial resolution (0.5mm×0.5mm) for ^{23}Na MRI of the rat head in the shortest time (21 minutes) to identify expected behavioral changes (Figures 2 and 3(d)). To the best of our knowledge, these are the highest quality ^{23}Na brain images achieved thus far of live rats.

To quantify sodium voxels, the standard curve with 0–200mM monosodium glutamate confirms that the ^{23}Na MRI voxel-intensity increments are linear (r^2=0.9949) in this volume RF coil. Regional sodium concentrations in the right (R) vitreous humor (108mM) and total brain (48mM) were derived using the linear regression equation. Our values in the total brain ROI are similar to the published rat brain value of 45±4mM (28); our value of the vitreous humor ROI is similar to published levels of human vitreous humor measured by ^{23}Na MRI of 113±14mM (29).

Serial ^{23}Na MR images of anesthetized rats were stable: subtraction of consecutive images taken over 4 hours did not change. Brain sodium did not change before or after saline injection, but increased distinctly after NTG. Figure 2(a) represents the sum of two consecutive 21-minute scans before saline injection and Figure 2(b) represents the sum of

two consecutive 21-minute scans in the same rat taken immediately after saline injection. Figure 2(c) represents the subtraction of 2(a) from 2(b). In these control experiments, the difference image, Figure 2(c), demonstrates no changes other than from eye movement. In the NTG experiments, Figure 2(d) represents the sum of three consecutive 21-minute scans before NTG injection and Figure 2(e) represents the sum of three consecutive 21-minute scans in the same rat taken immediately after NTG injection. Figure 2(f) represents the subtraction of 2(d) from 2(e). In Figure 2(f), the sodium is distinctly increased in the brain. The summing of scans in these experiments was employed to increase SNR; these difference changes after NTG were consistent in all 10 rats tested whether summing of two, three or six images was employed.

Scrolling the 7mm thick ^{23}Na MRI through the 0.4mm ^{1}H MRI slices, we identified features in the ^{23}Na MRI that best correlated with the anatomical structures in the rat head in the axial plane. Figure 3(a)–(c) shows three slices that illustrate the sites that constitute the most prominent structures in the 7mm thick ^{23}Na MRI slice. For quantitative study, we selected eight regions of interest (ROIs), outlined in Figure 3(d), as predominantly reflecting vitreous humor (R & L), frontal CSF, total brain, frontal brain (R & L), and posterior CSF (R & L).

ROI average voxel intensities from saline-injected control rats (n=3) were no different than non-injected controls (n=6). The quantified measures combined from both control groups (n=9: not injected, n=6, plus saline-injected, n=3) were normalized to 1 and compared to the corresponding ROIs from rats scanned 25 minutes (n=6), 145 minutes (n=6), and 3–4 days after NTG (n=3), as shown in Figure 3(e). The average voxel intensities in all ROIs at all time-points after NTG were significantly increased, p<0.05, Kruskal–Wallis test, two-tailed. At the time of the first MRI scans after NTG (25 minutes), sodium was elevated in all animals compared to controls. The specific ROI increases in sodium after NTG ranged from 7.5 to 17 % (Table 1), and included intracranial CSF, brain, and, unexpectedly, in vitreous humor – in spite of eye movement artifact. The apparently larger eyeball dimension is also consistent with eye movement. Sodium did not change in the extracranial muscles, which showed a minimal decrease of 3.6% after NTG (Table 1).

The temporal ^{23}Na MRI profile revealed that sodium was elevated at the time of the first measure, 25 minutes after NTG. The sodium increase was maintained in all eight regions at 145 minutes after NTG when the effect was more reproducible, as reflected in the smaller standard deviation, seen in Figure 3(e). Three animals were allowed to recover from anesthetic 3–4 hours after their first NTG injection; 3–4 days later they had normal eyelid separation and von Frey hair-withdrawal responses, and they interacted indistinguishably from other rats in their enclosures. When anesthetized and imaged a second time, their sodium had decreased to levels approaching those of injection- naïve rats, although Figure 3(e) shows that their regional sodium was still significantly higher than in control rats. At this time, the animals received a second NTG injection: Their sodium rose again to the same levels they had after the first NTG injection (data not shown).

Simulating neuronal excitability with extracellular sodium concentration ($[Na^+]_o$)

To study whether a rise in extracellular sodium would affect neuronal excitability, we simulated its effect on neuronal firing in a simple somatic model, where Na^+ current, leak current (including Na^+ conductance), sodium pump, and sodium diffusion contribute to a Na^+ kinetic change (see Methods and Appendix). The firing frequency in Figure 4(a) was 5.75 Hz in 160mM $[Na^+]_o$ (pink) and 3.25 Hz at 145mM (blue). Moreover, the action potential (AP) at 160mM $[Na^+]_o$ occurred earlier. These results are similar to the effects from changing $[Na^+]_o$ on the neuronal excitability of primary cultured neurons as studied by patch clamp (31).

One of the advantages of modeling is to study specific currents without blocking other channels in current- clamp mode. Thus we plotted the Na^+ and K^+ currents during current-clamp recordings: simulation shows Figure 4(b) and (c) that artificial CSF with 160mM $[Na^+]_o$ induces earlier Na^+ and K^+ currents than that with 145mM $[Na^+]_o$.

Because Na,K-ATPase is critical in maintaining a balance of $[Na^+]_i$ and $[Na^+]_o$, we changed the cellular Na,K-ATPase density to study its influence on the effects of $[Na^+]_o$ on APs. The AP frequency rate increase induced by $[Na^+]_o$ at 160 compared to 145mM is dependent on the density of neuronal Na,K-ATPase (Figure 4(d)). For example, increasing $[Na^+]_o$ from 145mM to 160mM increases the AP rate by 79% at a neuronal pump density of 2.2 $\mu A/cm^2$ but only by 27% when the density is 2.1 $\mu A/cm^2$. The density of 2.2 $\mu A/cm^2$ used in our modeling is within published physiological ranges (31–34).

To identify the firing frequency over a broad range of $[Na^+]_o$ in Figure 4(e), we found that the model neuron fires faster when $[Na^+]_o$ rises above 130mM. The vertical line b in Figure 4(e) shows that the 17% increase we found in the ^{23}Na MRI of sensitized rats (equivalent to ~165mM $[Na^+]_o$) produces a higher firing frequency of 6.38 Hz.

Discussion

The major finding in this study is that allodynia (hindpaw sensitivity) and photophobia (eye squinting) occur within 1 hour after NTG, synchronous with a significant increase in sodium as measured in vivo using ultra-high field ^{23}Na MRI, and the sodium rise increases the spontaneous neuronal excitability by more than 1.75-fold in simulation studies. These are the first observations of these events. From these results, we propose a localizing mechanism to account for the increased neuronal excitability that underlies the allodynia and photophobia of migraine.

Neuronal excitation and migraine

One of the central neurobiological events in migraine is widespread neuronal excitation, yet its genesis is not known. While animal models cannot replicate many aspects of human pain (35), the work of others with the NTG rat (19,20,35) supports this as a useful migraine model. An important mechanistic insight from our data is that the observed rise in sodium may directly increase neuronal excitation at multiple locations of established importance in migraine. For instance, increased trigeminal nociceptor activation is postulated to generate the characteristic pain of migraine (8,9,37), but the source of activation is not known; we propose that increased sodium in the CSF that perfuses these nociceptors directly increases their excitability. In another example, intrinsically photosensitive retinal ganglion cells are involved in a pathway for photophobia (4), but the source of their activation is not known; our observations of eye squinting suggest photophobia as early as 40–45 minutes after NTG injection, and we propose that the increased sodium we observe in vitreous humor as early as 25 minutes after NTG directly increases the excitability of retinal neurons that may contribute to photophobia. Migraineurs frequently describe sensations like an ice pick in their eye (38); we propose that elevated vitreous humor sodium causes excitatory neurons to fire faster than inhibitory neurons, possibly because of different Na,K-ATPase densities (Figure 4(d)), resulting in a net hyper-excitability that contributes to the source of this severe photophobia.

Our ^{23}Na MRI data in this rat migraine model correlates with other characteristics of migraine. Prolonged peripheral and central sensitization, well recognized in migraine and animal pain studies, are reflected in Figure 3(e) with the persistence of mild sodium elevation several days after central sensitization was triggered. Elevated sodium around cranial nerve roots and in the brain has potential to directly change neuronal excitation with

varied consequences – focal or widespread. These include phonophobia, ophthalmo-plegia, confusion, and disturbed sleep. It will, therefore, be of interest to study Na MRI during acute, interictal, and chronic migraine states.

Where does sodium change and how?

In our experiments, ^{23}Na MRI measures total sodium and the spatial resolution cannot distinguish intracellular from extracellular compartments. Possible sources of the increased [Na^+] include brain, CSF, or blood. Because intracellular sodium is negligible, sodium MRI mainly reflects $[Na^+]_o$. There is no evidence of any decrease in the ^{23}Na MRI observed in the subtraction images. Previous lumbar CSF and blood plasma data from migraineurs has shown that sodium changed in the CSF not the blood, and that there was no concentration effect, because CSF osmolarity was unchanged (13). The accumulating evidence suggests that a specific increase in net [Na^+] is occurring. This might arise if more sodium entered the intracranial and ocular fluids from the blood supply, or less was removed into the venous drainage; further studies may investigate these possibilities. We proposed that brain capillary endothelial cell Na,K-ATPase (typically the alpha-2 isoform) is the principal regulator of CSF and brain sodium (39), and intra-orbital sodium is primarily regulated in the rat-ciliary epithelium by the alpha-2 isoform of the Na,K-ATPase (40). Thus increased Na,K-ATPase activity on the supply side and/or decreased Na,K-ATPase activity on the drainage side might be involved. There is extensive potential to alter Na,K-ATPase in migraine because many regulators of Na,K-ATPase, such as serotonin, adrenaline, and estrogen (39), are also known to be involved in migraine.

NTG injection triggers the increase in sodium as neither isoflurane anesthesia nor saline injection resulted in any sodium shift. While NTG is a potent vasodilator, the sodium increase is not a direct effect because vasodilation has a rapid onset and decline, with a half-life of around 2 minutes. The mechanism whereby NTG triggers central sensitization and migraine remains to be fully delineated (41,42). The nitric oxide donor function of NTG up-regulates cyclic GMP signal transduction pathways (36,43) and treatment with nitric oxide synthase inhibitors blocks this effect, suggesting endothelial nitric oxide synthase involvement (41). Our theory (39) emphasizes that many migraine-related molecules are known to regulate Na,K-ATPase on the abluminal side of brain capillary endothelial cells via cyclic GMP pathways, including nitric oxide. NTG affects Na,K-ATPase, mainly through cGMP, but with conflicting isoform- and tissue-specific inhibition or activation effects (44,45).

Limitations of the study

As described in the Methods section, the 2D imaging with 7mm deep slabs restricts our interpretation of precise structural identifications on the ^{23}Na images. We are currently developing 3D sequences to overcome this shortcoming.

At the cellular level, the brain has a large variety of cells – including excitatory and inhibitory neurons, glia, immune, and mast cells – that have different functions and interact with each other in the form of functional units or networks: higher [Na^+] might have different effects on different cell types, and we have not studied these effects in our simulations. The complexities of these different neurotransmission and cellular responses demonstrate the need to further test our interpretation that increased sodium at migraine neuronal pathways increases neuronal excitability.

The substantial increase in sodium after NTG provides a much-needed objective measure for further studies in this migraine model, but our observations need to be replicated by others, the spatial resolution of the ^{23}Na MRI needs to be further evaluated with different sequences

and in three dimensions, and to discover if it responds to anti-migraine treatments. For instance, it will be of interest to see whether anti-migraine therapy that protects against the central sensitization in this model will also reverse the NTG-induced elevation in sodium. Finally, the mechanisms behind the altered sodium need to be investigated.

Future directions

The rat model may not represent events in spontaneous migraine. In addition to the aforementioned animal model studies, future work could include in vivo human studies of migraine when improved sensitivity of ^{23}Na MRI becomes available (46). The ability to demonstrate sodium changes in vivo at levels that can change neuronal excitability provides an alternative to BOLD fMRI. BOLD fMRI studies of migraine typically yield an MRI signal change of a few percent lasting for several minutes (6), whereas the ^{23}Na MRI changes observed here ranged up to 17% and stayed at this level for over 2 hours, more in line with the migraine phenotype.

The advent of high-field human MRI scanners allows for ^{23}Na imaging as high as 9.4 T, which increases MRI signal by several fold compared to the 3 T MRI scanners widely available in clinical practice. The sodium image quality is dramatically improved at 9.4 T compared to 3 T (47) and we speculate that clinical translation of the findings presented here is feasible. However, 7 T and 9.4 T MRI scanners are expensive, not widely available, and not yet approved by the US FDA and European regulators for human clinical diagnosis. An attractive alternative is to take advantage of the low resonant frequency of ^{23}Na, and combine existing 1.5 T (ω_{23Na}=17 MHz) or 3 T (ω_{23Na}=34 MHz) MRI technology with high-temperature superconductive (HTS) RF coils. HTS technology increases SNR by decreasing noise preferentially and works best in the low MR frequency range. Preliminary results (Time Medical, Metuchen, NJ) are encouraging with 3- to 4-fold sensitivity enhancement using conventional copper conductor technology that may enable the quality of ^{23}Na MR images at 3 T to approach those achieved at 7 T or 9.4 T.

Concluding remarks

Behavioral measures of allodynia and photophobia occur within 1 hour of NTG injection in the rat migraine model. In the same time-frame, we find that brain, intracranial CSF, and vitreous humor [Na^+] increase between 7.5 and 17% by using high-resolution, high-sensitivity ^{23}Na MRI sequences. These sodium elevations are sufficient to increase neuronal excitability by more than 1.75-fold in simulated neurons. We propose that increasing sodium at the locations of neuronal pathways involved in migraine increases the neuronal excitability that underlies the pain and photophobia of migraine. We discuss a strategy to test whether these findings can be extended to human ^{23}Na MRI.

Acknowledgments

A portion of this work was performed at the National High Magnetic Field Laboratory, which is supported by the National Science Foundation Cooperative Agreement No. DMR-0654118, the State of Florida, and the US Department of Energy. We thank Russ Jacobs at Caltech for help with imaging software.

Funding

This work was supported by grants from the National Institutes of Health RO1 NS-043295, R21 CA119177, and the Norris, Glide, and Lucas Brothers Foundations.

References

1. Lipton RB, Scher AI, Kolodner K, et al. Migraine in the United States: epidemiology and patterns of health care use. Neurology. 2002; 58:885–894. [PubMed: 11914403]

2. Lance JW, Anthony M. Some clinical aspects of migraine. A prospective survey of 500 patients. Arch Neurol. 1966; 15:356–361. [PubMed: 5912494]
3. Goadsby PJ, Charbit AR, Andreou AP, et al. Neurobiology of migraine. Neuroscience. 2009; 161:327–341. [PubMed: 19303917]
4. Noseda R, Kainz V, Jakubowski M, et al. A neural mechanism for exacerbation of headache by light. Nat Neurosci. 2010; 13:239–245. [PubMed: 20062053]
5. Lauritzen M, Olesen J. Regional cerebral blood flow during migraine attacks by Xenon-133 inhalation and emission tomography. Brain. 1984; 107(Pt 2):447–461. [PubMed: 6609739]
6. Hadjikhani N, Sanchez Del Rio M, Wu O, et al. Mechanisms of migraine aura revealed by functional MRI in human visual cortex. Proc Natl Acad Sci U S A. 2001; 98:4687–4692. [PubMed: 11287655]
7. Burstein R, Yamamura H, Malick A, et al. Chemical stimulation of the intracranial dura induces enhanced responses to facial stimulation in brain stem trigeminal neurons. J Neurophysiol. 1998; 79:964–982. [PubMed: 9463456]
8. Bolay H, Reuter U, Dunn AK, et al. Intrinsic brain activity triggers trigeminal meningeal afferents in a migraine model. Nat Med. 2002; 8:136–142. [PubMed: 11821897]
9. Zhang X, Levy D, Noseda R, et al. Activation of meningeal nociceptors by cortical spreading depression: implications for migraine with aura. J Neurosci. 2010; 30:8807–8814. [PubMed: 20592202]
10. Iadecola C. From CSD to headache: a long and winding road. Nat Med. 2002; 8:110–112. [PubMed: 11821889]
11. de Vries B, Frants RR, Ferrari MD, et al. Molecular genetics of migraine. Hum Genet. 2009; 126:115–132. [PubMed: 19455354]
12. Jen JC, Kim GW, Dudding KA, et al. No mutations in CACNA1A and ATP1A2 in probands with common types of migraine. Arch Neurol. 2004; 61:926–928. [PubMed: 15210532]
13. Harrington MG, Fonteh AN, Cowan RP, et al. Cerebrospinal fluid sodium increases in migraine. Headache. 2006; 46:1128–1135. [PubMed: 16866716]
14. Cserr HF, Depasquale M, Patlak CS, et al. Convection of cerebral interstitial fluid and its role in brain volume regulation. Ann N Y Acad Sci. 1986; 481:123–134. [PubMed: 3468852]
15. Davson H, Pollay M. The turnover of 24Na in the cerebrospinal fluid and its bearing on the blood-brain barrier. J Physiol. 1963; 167:247–255. [PubMed: 14025546]
16. Kirsch S, Augath M, Seiffge D, et al. In vivo chlorine-35, sodium-23 and proton magnetic resonance imaging of the rat brain. NMR Biomed. 2010; 23:592–600. [PubMed: 20232452]
17. Schepkin VD, Brey WW, Gor'kov PL, et al. Initial in vivo rodent sodium and proton MR imaging at 21. 1 T. Magn Reson Imaging. 2010; 28:400–407. [PubMed: 20045599]
18. Gor'kov PLQC, Beck BL, Clark M, et al. A modular MRI probe design for large rodent neuroimaging at 21. 1 T (900 MHz). Proc Intl Soc Mag Reson Med. 2009; 17:2952.
19. Di Clemente L, Coppola G, Magis D, et al. Nitroglycerin sensitises in healthy subjects CNS structures involved in migraine pathophysiology: evidence from a study of nociceptive blink reflexes and visual evoked potentials. Pain. 2009; 144:156–161. [PubMed: 19457613]
20. Tassorelli C, Joseph SA. Systemic nitroglycerin induces Fos immunoreactivity in brainstem and forebrain structures of the rat. Brain Res. 1995; 682:167–181. [PubMed: 7552308]
21. Pardutz A, Krizbai I, Multon S, et al. Systemic nitroglycerin increases nNOS levels in rat trigeminal nucleus caudalis. Neuroreport. 2000; 11:3071–3075. [PubMed: 11043526]
22. de Tommaso M, Libro G, Guido M, et al. Nitroglycerin induces migraine headache and central sensitization phenomena in patients with migraine without aura: a study of laser evoked potentials. Neurosci Lett. 2004; 363:272–275. [PubMed: 15182958]
23. Paxinos, G.; Watson, C. The Rat Brain in Stereotaxic Coordinates. London: Academic Press; 2007.
24. Fu R, Brey WW, Shetty K, et al. Ultra-wide bore 900 MHz high-resolution NMR at the National High Magnetic Field Laboratory. J Magn Reson. 2005; 177:1–8. [PubMed: 16125429]
25. Hines ML, Carnevale NT. The NEURON simulation environment. Neural Comput. 1997; 9:1179–1209. [PubMed: 9248061]

26. Migliore M, Hoffman DA, Magee JC, et al. Role of an A-type K+ conductance in the back-propagation of action potentials in the dendrites of hippocampal pyramidal neurons. J Comput Neurosci. 1999; 7:5–15. [PubMed: 10481998]
27. Canavier CC, Landry RS. An increase in AMPA and a decrease in SK conductance increase burst firing by different mechanisms in a model of a dopamine neuron in vivo. J Neurophysiol. 2006; 96:2549–2563. [PubMed: 16885519]
28. Christensen JD, Barrere BJ, Boada FE, et al. Quantitative tissue sodium concentration mapping of normal rat brain. Magn Reson Med. 1996; 36:83–89. [PubMed: 8795025]
29. Ouwerkerk R, Bleich KB, Gillen JS, et al. Tissue sodium concentration in human brain tumors as measured with 23Na MR imaging. Radiology. 2003; 227:529–537. [PubMed: 12663825]
30. Arakaki X, Foster H, Su L, et al. Extracellular sodium modulates the excitability of cultured hippocampal pyramidal cells. Brain Res. In press.
31. Shen KZ, Johnson SW. Sodium pump evokes high density pump currents in rat midbrain dopamine neurons. J Physiol. 1998; 512(Pt 2):449–457. [PubMed: 9763634]
32. Wang HY, Huang RC. Diurnal modulation of the Na+/K+-ATPase and spontaneous firing in the rat retinorecipient clock neurons. J Neurophysiol. 2004; 92:2295–2301. [PubMed: 15381747]
33. Despa S, Bers DM. Functional analysis of Na+/K+-ATPase isoform distribution in rat ventricular myocytes. Am J Physiol Cell Physiol. 2007; 293:C321–C327. [PubMed: 17392375]
34. Dobretsov M, Hastings SL, Stimers JR. Functional Na+/K+ pump in rat dorsal root ganglia neurons. Neuroscience. 1999; 93:723–729. [PubMed: 10465456]
35. Mogil JS. Animal models of pain: progress and challenges. Nat Rev Neurosci. 2009; 10:283–294. [PubMed: 19259101]
36. Tassorelli C, Blandini F, Greco R, et al. Nitroglycerin enhances cGMP expression in specific neuronal and cerebrovascular structures of the rat brain. J Chem Neuroanat. 2004; 27:23–32. [PubMed: 15036360]
37. Levy D, Burstein R, Kainz V, et al. Mast cell degranulation activates a pain pathway underlying migraine headache. Pain. 2007; 130:166–176. [PubMed: 17459586]
38. Lance JW. Fifty years of migraine research. Aust N Z J Med. 1988; 18:311–317. [PubMed: 3056372]
39. Harrington MG, Fonteh AN, Arakaki X, et al. Capillary endothelial Na(+), K(+), ATPase transporter homeostasis and a new theory for migraine pathophysiology. Headache. 2010; 50:459–478. [PubMed: 19845787]
40. Wetzel RK, Sweadner KJ. Immunocytochemical localization of NaK-ATPase isoforms in the rat and mouse ocular ciliary epithelium. Invest Ophthalmol Vis Sci. 2001; 42:763–769. [PubMed: 11222539]
41. Greco R, Meazza C, Mangione AS, et al. Temporal profile of vascular changes induced by systemic nitroglycerin in the meningeal and cortical districts. Cephalalgia. 2011; 31:190–198. [PubMed: 20693231]
42. Christiansen I, Iversen HK, Olesen J, et al. Nitric oxideinduced headache may arise from extracerebral arteries as judged from tolerance to isosorbide-5-mononitrate. J Headache Pain. 2008; 9:215–220. [PubMed: 18521538]
43. Behrends S, Knyihar-Csillik E, Kempfert J, et al. Glyceryl trinitrate treatment up-regulates soluble guanylyl cyclase in rat dura mater. Neuroreport. 2001; 12:3993–3996. [PubMed: 11742226]
44. Pontiggia L, Winterhalter K, Gloor SM. Inhibition of Na,K-ATPase activity by cGMP is isoform-specific in brain endothelial cells. FEBS Lett. 1998; 436:466–470. [PubMed: 9801170]
45. McKee M, Scavone C, Nathanson JA. Nitric oxide, cGMP, and hormone regulation of active odium transport. Proc Natl Acad Sci U S A. 1994; 91:12056–12060. [PubMed: 7527549]
46. Atkinson IC, Sonstegaard R, Pliskin NH, et al. Vital signs and cognitive function are not affected by 23- sodium and 17-oxygen magnetic resonance imaging of the human brain at 9. 4 T. J Magn Reson Imaging. 2010; 32:82–87. [PubMed: 20578014]
47. Inglese M, Madelin G, Oesingmann N, et al. Brain tissue sodium concentration in multiple sclerosis: a sodium imaging study at 3 tesla. Brain. 2010; 133:847–857. [PubMed: 20110245]

Appendix

Equations used in the modeling studies

Sodium current:

$$I_{Na}=0.01*m^3*h*i*(v-E_{Na})$$
$$m_\infty=\frac{\alpha_m}{(\alpha_m+\beta_m)};\tau_m=\frac{1}{(\alpha_m+\beta_m)}$$
$$\alpha_m=\frac{0.4*(v+30)}{(1-e^{(-(v+30)/7.2)})}$$
$$\beta_m=\frac{0.124*(v+30)}{(e^{((v+30)/7.2)}-1)}$$
$$h_\infty=\frac{1}{(1+e^{((v+50)/4)})}$$
$$\tau_h=\frac{1}{\alpha_h+\beta_h}$$
$$\alpha_h=\frac{0.03*(v+45)}{(1-e^{(-(v+45)/1.5)})}$$
$$\beta_h=\frac{0.01*(v+45)}{e^{\frac{v+45}{1.5}}-1}$$
$$i_\infty=\frac{1+\left(0.8*e^{\left(\frac{v+58}{2}\right)}\right)}{1+e^{\left(\frac{v+58}{2}\right)}}$$
$$\tau_i=\frac{3*10^4*\beta_i}{1+\alpha_i}$$
$$\alpha_i=e^{(0.469*(v+60))}$$
$$\beta_i=e^{(0.094*(v+60))}$$

If τ_m<0.02, then τ_m=0.02 ms;

If τ_h<0.5, then τ_h=0.5 ms;

If τ_i<10, then τ_i=10 ms.

K_{DR} current:

$$I_{K_{DR}}=0.003*n*(v+90)$$
$$n_\infty=\frac{1}{1+\alpha_n};\tau_n=\frac{50*\beta_n}{1+\alpha_n}$$
$$\alpha_n=e^{(-0.117*(v-13))}$$
$$\beta_n=e^{(-0.082*(v-13))}$$

If τ_n<2, then τ_n=2 ms.

K_A current:

$$I_{K_A}=0.008*n*l*(v+90)$$
$$n_\infty=\frac{1}{1+\alpha_n};\tau_n=\frac{20*\beta_n}{1+\alpha_n}$$
$$\alpha_n=e^{\left(-0.039*\left(1.5+\frac{1}{1+e^{\frac{(v+40)}{5}}}\right)*(v-11)\right)}$$
$$\beta_n=e^{\left(-0.021*\left(1.5+\frac{1}{1+e^{\frac{(v+40)}{5}}}\right)*(v-11)\right)}$$
$$l_\infty=\frac{1}{1+\alpha_l};\tau_1=0.26*(v+50)$$
$$\alpha_l=e^{(0.117*(v+56))}$$

If τ_n<0.1, then τ_n=0.1 ms;

If $\tau_l<2$, then $\tau_l=2$ ms.

Sodium pump current:

$$I_{NaP,i}=\frac{0.0022}{1+\left(\frac{10}{[Na]_i}\right)^{1.5}}$$
$$I_{Na}=3*I_{NaP,i};I_K=-2*I_{NaP,i}$$

Sodium diffusion:

$$\frac{\mathrm{d}[Na]_i}{dt}=\frac{4*(-I_{Na}-I_{L,Na}-3*I_{NaP})}{d*F}$$

Linear leak current:

$$I_L=I_{L,Na}+I_{L,K};I_{L,k}=g_{L,K}*(V-E_K);$$
$$I_{L,Na}=g_{L,Na}*(V-E_{Na});$$
$$E_{Na}=\frac{RT}{F}*\mathrm{In}\left(\frac{[Na]_o}{[Na]_i}\right)$$

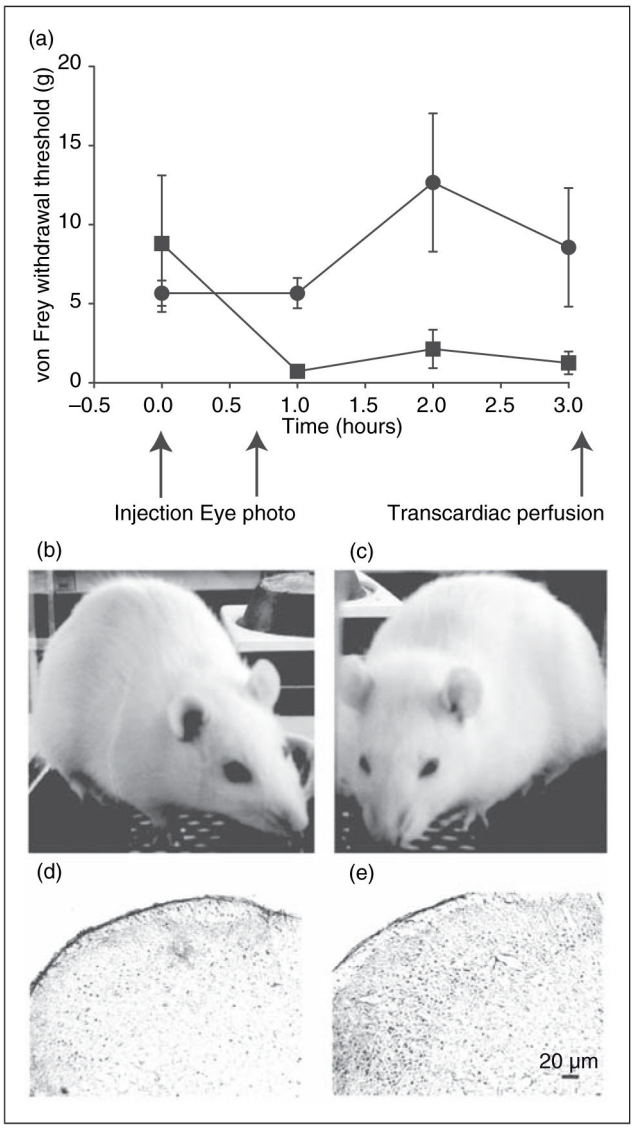

Figure 1.

Behavioral and immunohistochemical measures of the NTG rat model. (a) The threshold of von Frey hair for hindpaw withdrawal is displayed (mean ± SD) for NTG-treated (solid squares; n=5) and control rats (solid circles; n=5) after baseline acclimation. Indicated are the times of NTG or saline injection, eye photography, and transcardiac perfusion. (b) Saline and (c) NTG-treated rat representative of the consistent eye-squinting behavior. The vertical height:width ratio of the eyelids in three saline-treated rats was greater than those of three NTG-treated animals, p<0.0001, two-tailed t-test. (d) cFos expression in 40 μm thick sections of the lower brain stem showing the trigeminal nucleus caudalis (TNC) area, Sp5C[41], after saline injection. (e) cFos expression in the TNC after NTG. Negative controls without primary cFos antibody had minimal cellular stain (data not shown).

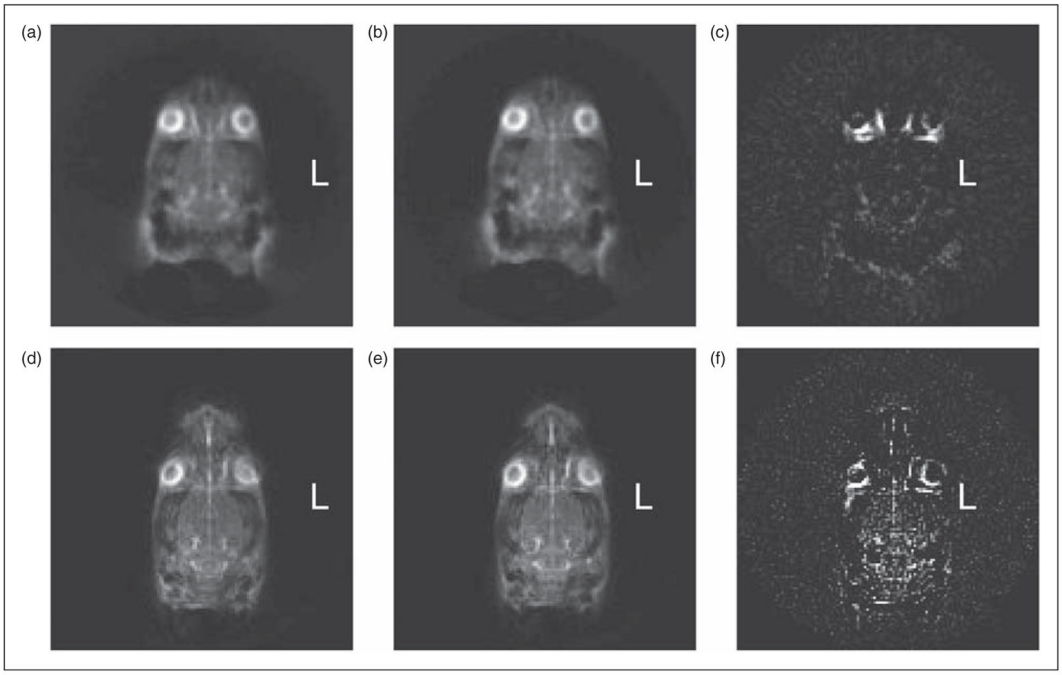

Figure 2.

Axial ^{23}Na MRI images of the rat head before and after central sensitization. (a) Sum of two 21-minute ^{23}Na MRI axial scans of a control rat. (b) Sum of two further scans immediately after saline injection in the same animal. (c) Difference in voxel intensity (b)–(a). (d) Sum of three 21-minute ^{23}Na MRI axial scans of another animal; (e) Sum of three further scans immediately after NTG injection in the same animal. (f) Difference in voxel intensity (e)–(d). This demonstrates the distinct increase in sodium as a consequence of NTG injection.

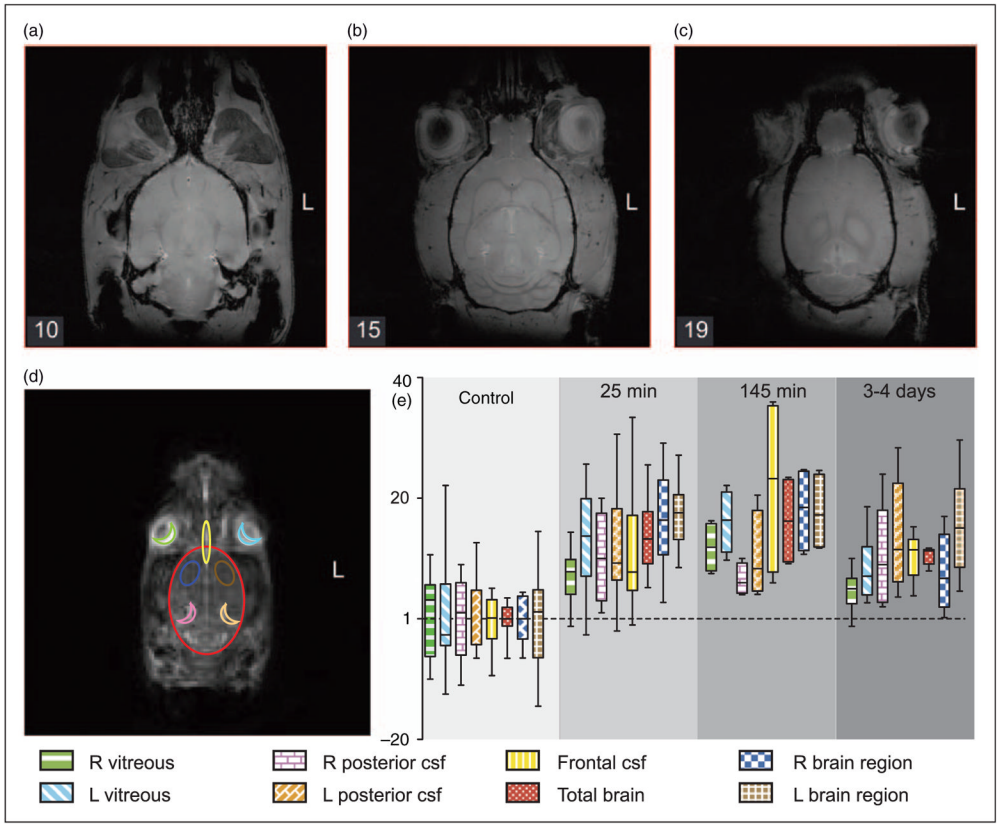

Figure 3.

Rat anatomy and quantitative changes in ^{23}Na MRI after NTG. (a), (b) and (c) are high-resolution (0.133mm×0.133mm×0.4 mm) axial-plane ^{1}H MRI slices of a representative rat head to identify anatomy from the 10th, 15th and 19th slice from base to top of the head. (d) shows an axial ^{23}Na MRI slice with outlines of eight selected ROIs for regional quantification (e), color and fill-coded as in the foot of the legend: vitreous humor (R & L), frontal CSF, frontal brain (R & L), total brain, and posterior CSF (R & L). Plot (e) shows means and standard deviations of the average voxel intensities in eight ROIs. NTG significantly increased sodium, $p<0.05$, Kruskal–Wallis test, two-tailed.

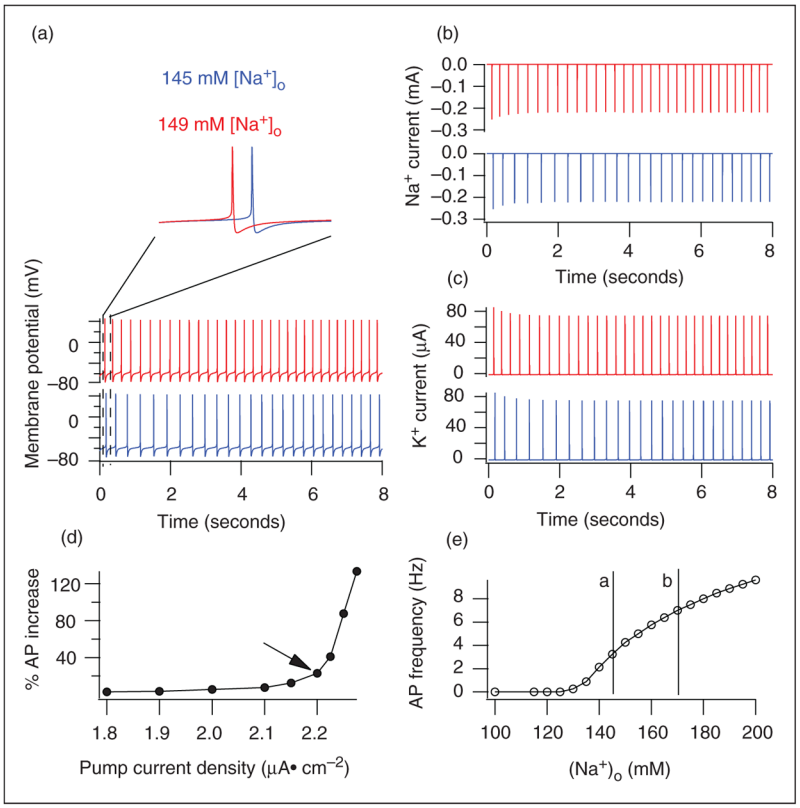

Figure 4.

Simulating the effects of extracellular sodium concentration, $[Na^+]_o$, on neuronal firing in a simple neuron soma built in NEURON (equations are in the Methods). (a) The earlier AP (pink) at $[Na^+]_o$ of 160 mM, and the faster firing rate when $[Na^+]_o$ is increased from 145 to 160 mM. (b) The sodium current peaks earlier in 160mM $[Na^+]_o$ (pink) compared to that in 145mM $[Na^+]_o$ (blue). (c) The potassium current peaks earlier in 160mM $[Na^+]_o$ (pink) compared to that in 145mM $[Na^+]_o$ (blue). (d) When $[Na^+]_o$ increases from 145 to 160 mM, the change in the firing rate was plotted against Na,K-ATPase density and revealed that the altered AP rate increased more distinctly above an Na,K-ATPase density of 2.1 μA/cm ^{2}. An Na,K-ATPase density of 2.2 μA/cm ^{2} (arrow) was used in all of our other simulations. (e) With $[Na^+]_o$ between 100 and 200mM and Na,K-ATPase density of 2.2 μA/cm ^{2}, the firing rate of the model neuron increased when $[Na^+]_o$ reached 130 mM. The lines a and b represent the range between normal and the 17% increase in sodium observed in the ^{23}Na MRI studies after NTG.

Table 1

Percent change of regional sodium concentration after NTG

Region	Controls (n=6, measured twice) RAVI × 10^7 (SD)	NTG (n=6, measured twice) RAVI × 10^7 (SD)	% Δ	P value
L vitreous humor	16.0 (1.1)	17.2 (0.7)	7.5 %	0.015
R vitreous humor	11.3 (1.1)	12.7 (1)	12 %	0.008
Frontal CSF	7.9 (0.3)	8.8 (0.9)	11 %	0.002
L front brain	4.8 (0.2)	5.6 (0.4)	17 %	0.002
R front brain	4.4 (0.4)	5.1 (0.3)	16 %	0.002
Total brain	5.8 (0.2)	6.6 (0.4)	14 %	<0.0001
L posterior CSF	10.0 (0.6)	11 (0.7)	10 %	0.021
R posterior CSF	8.9 (0.6)	9.9 (0.9)	11 %	0.011
R & L jaw muscle	2.9 (0.6)	2.8 (0.7)	−3.6 %	0.240

RAVI=regional average voxel intensity; SD=standard deviation; P values for specific regional comparisons using Dunn's Multiple Comparison Test.